

Observations of Seismicity and Ground Motion in the Northeast U.S. Atlantic Margin from Ocean-Bottom Seismometer Data

by **Claudia H. Flores, Uri S. ten Brink, Jeffrey J. McGuire, and John A. Collins**

ABSTRACT

Earthquake data from two short-period ocean-bottom seismometer (OBS) networks deployed for over a year on the continental slope off New York and southern New England were used to evaluate seismicity and ground motions along the continental margin. Our OBS networks located only one earthquake of $M_c \sim 1.5$ near the shelf edge during six months of recording, suggesting that seismic activity ($M_{Lg} > 3.0$) of the margin as far as 150–200 km offshore is probably successfully monitored by land stations without the need for OBS deployments. The spectral acceleration from two local earthquakes recorded by the OBS was found to be generally similar to the acceleration from these earthquakes recorded at several seismic stations on land and to hybrid empirical acceleration relationships for eastern North America. Therefore, the seismic attenuation used for eastern North America can be extended in this region at least to the continental slope. However, additional offshore studies are needed to verify these preliminary conclusions.

Electronic Supplement: Tables of ocean-bottom seismometer (OBS) locations with recording start and end times, list of earthquakes on land used to identify the detection limits of OBSs, and station information, figures of probability density functions (PDFs) and waveforms, and zip archive of waveform data.

INTRODUCTION

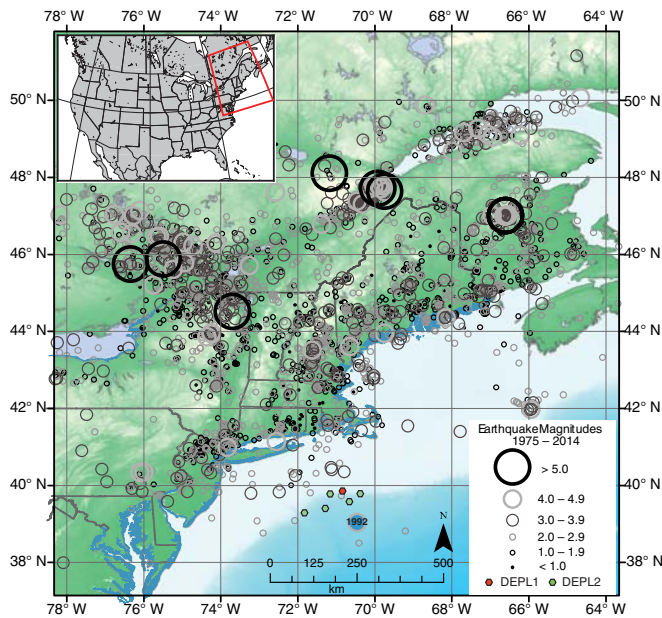
This study seeks to estimate the earthquake activity and seismic attenuation along one segment of the U.S. Atlantic margin by analyzing seismic data recorded by two temporary networks of ocean-bottom seismometers (OBSs) on the continental slope off New York and New England. To our knowledge, this is the first ever attempt to evaluate these parameters directly on the U.S. Atlantic margin.

Continental margins are boundary zones between continental and oceanic crusts and lithospheres. They have been

subjected to tectonic and magmatic activity during their formation, and thus their structure may be quite heterogeneous and is likely transitional between oceanic and continental crusts. Continental margins also store many of the thickest sedimentary packages on Earth, as much as 15 km offshore the mid-Atlantic states (e.g., Poag and Sevon, 1989). These two characteristics of the shallow structure of the continental margin, namely heterogeneity and thick sediments, suggest that the attenuation of seismic energy within the continental margin cannot be *a priori* extrapolated from either the continental or the oceanic crust.

The detection by land seismometers of several continental margin earthquakes with magnitudes of M_{Lg} 2.0–4.0 in this region during the years 2008–2011 motivated the deployment of the OBS networks in 2012 and 2013. The offshore region is not seismically quiescent, as evident from the 22 August 1992 M_{Lg} 4.8 earthquake offshore New Jersey (Kim, 1998). Further motivation for the study was the recent realization of tsunami potential from landslides along the margin. If these landslides are primarily generated by earthquake ground motion, then seismic attenuation may govern the size and distribution of earthquake-generated landslides and needs to be quantified for accurate hazard models.

Hundreds of landslide scars were mapped along the U.S. Atlantic margin (Chaytor *et al.*, 2009; ten Brink *et al.*, 2014). Using Monte Carlo simulations, ten Brink, Barkan, *et al.* (2009) reproduced the observed cumulative landslide area distribution on the margin with two simple assumptions: (1) infinite slope stability analysis that determines the acceleration needed to displace seafloor sediments, and (2) horizontal acceleration for which amplitude and attenuation with distance from the rupturing fault depend on earthquake magnitude. To calculate the maximum landslide area as a function of the magnitude of the triggering earthquake, ten Brink, Lee, *et al.* (2009) used the Campbell (2003) and Tavakoli and Pezeshk (2005) peak spectral acceleration (PSA) curves for the eastern United States, because attenuation relationships for the margin were unknown. The good fit between the calculated and observed cumulative distri-



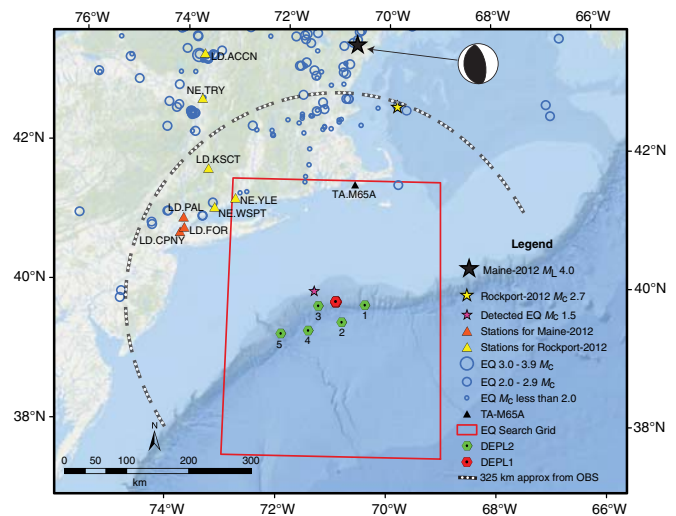
▲ **Figure 1.** Weston Observatory Network Seismicity. Location map of cataloged earthquakes between 1975 and 2014 from the New England Seismic Network (NESN). Modified from the original map (see [Data and Resources](#)). Grayscale coding of symbols is used to distinguish magnitude size. Earthquake depths range from 0 to 38 km. Hexagons show location of DEPL1 and DEPL2. Event labeled 1992 is the M_{Lg} 4.8 earthquake from [Kim \(1998\)](#). Inset, map of the United States showing boxed area of interest. The color version of this figure is available only in the electronic edition.

butions of observed landslides along the Atlantic margin and that calculated from slope stability analysis suggests that landslide area can be related to earthquake magnitude ([ten Brink, Barkan, et al., 2009](#)). Therefore, earthquake probability could be used to predict submarine landslide probability. In this study, we attempt to glean information about ground motions from OBSs deployed at the continental margin to help refine predicted submarine landslide probability for the U.S. East Coast.

Figure 1 shows earthquake activity for the northeastern U.S. region from the years 1975 to 2014 from the New England Seismic Network (NESN) catalog (see [Data and Resources](#)). Although seismic activity has been detected along the mid-Atlantic and New England portions of the margin, a reliable probabilistic estimate of earthquake activity in the continental margin does not exist. [Peterson et al. \(2014\)](#) extended the contours of their probabilistic estimate of spectral acceleration (SA) from the continental United States into the proximal shelf, although they lacked constraints offshore. Nevertheless, the extended SA offshore was used to estimate the probability and amplitude of a landslide-generated tsunami along the U.S. Atlantic coast (e.g., [Grilli et al., 2009](#)).

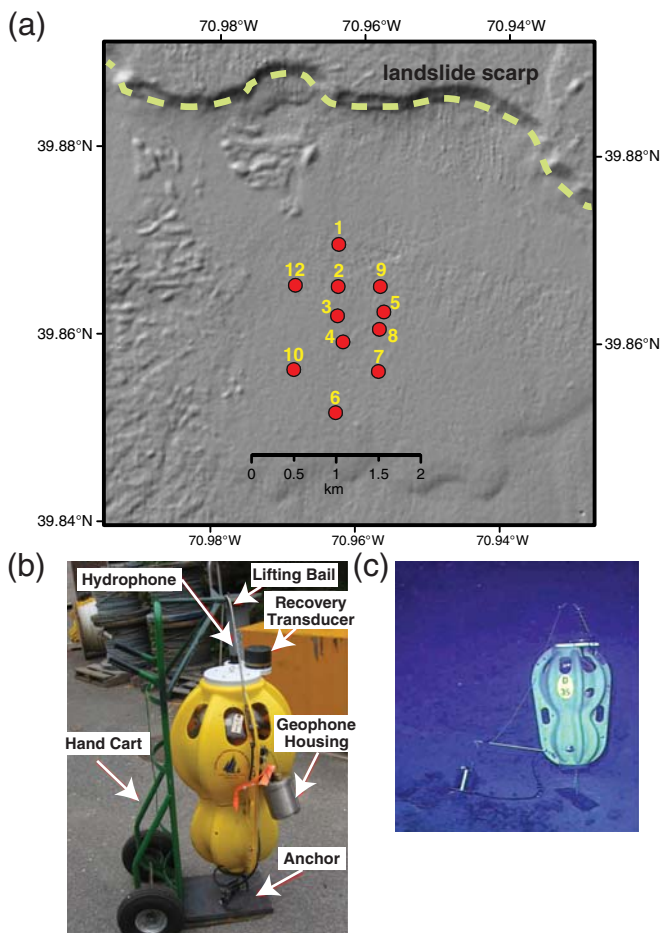
DATA

Two OBS deployments were carried out in succession from June 2012 to August 2013 along the eastern U.S. continental



▲ **Figure 2.** Location map of the study area. Open circles show earthquakes that occurred during both DEPL1 and DEPL2 from July 2012 to May 2013. Hexagons show the ocean-bottom seismometer (OBS) locations for DEPL1 and DEPL2. The dashed arc is centered on DEPL1 with a radius of 325 km and shows the extent at which a crustal M_c 2.7 earthquake can be detected by the OBS. The rectangle outlines the area used to search for potential local earthquakes detected by DEPL2. Triangles are labeled using the International Federation of Digital Seismograph Network and station codes. They show on-land stations used in this study. NE, New England Seismic Network; LD, Lamont-Doherty Cooperative Seismographic Network; and TA, USArray. Stars indicate events discussed in detail. The focal mechanism plot shows the 2012 Maine earthquake (NP1 = strike 384° , dip 61° , rake 84° ; NP2 = strike 180° , dip 30° , rake 100°) from the Saint Louis University Digital Focal Mechanism website (see [Data and Resources](#)). The color version of this figure is available only in the electronic edition.

margin within ~ 200 km from the southern New England (SNE) coastline (Figs. 2 and 3a). Table S1 (available in the electronic supplement to this article) lists both deployment OBS geographical locations and their water depths. The instruments used were short-period “D2s” from the Woods Hole Oceanographic Institution’s (WHOI’s) fleet that is part of the National Science Foundation’s Ocean-Bottom Seismograph Instrument Pool (OBSIP; see [Data and Resources](#)). Each D2 OBS consist of gimbaled three-orthogonal component short-period seismometers, a Geospace GS-11D 4.5 Hz geophone, and a High Tech HTI-90-U hydrophone with a low-frequency corner at 5 Hz. The Quanterra Q330 data logger was set at a sample rate of 100 Hz. An example of a D2 instrument is shown in Figure 3b. A complete list of specifications on the WHOI D2 can be found in the OBSIP website. OBS deployments are limited by the lack of control over instrument placement and coupling on the seafloor, and by the lack of clock synchronization with Global Positioning System during deployment. In addition, instruments may be susceptible to bottom ocean currents generating tilt noise ([Duennebier and Sutton,](#)



▲ **Figure 3.** (a) Detailed location of DEPL1 (labeled DEPL1 hexagons in Fig. 2) plotted over high-resolution shaded relief of the bathymetry from Andrews *et al.* (2013). The dashed line is an identified landslide scarp. (b) Image of Woods Hole Oceanographic Institution (WHOI) D2 instrument used in both OBS deployments with major components labeled. Image adapted from original located at Ocean-Bottom Seismograph Instrument Pool website (see Data and Resources). (c) Image of WHOI D2 as it sits deployed on the seafloor. In this photo, the geophone is not well coupled to the seafloor due to the rocky nature of the seafloor. This photo was taken from a different OBS deployment than the one discussed in this article. Image courtesy of WHOI. The color version of this figure is available only in the electronic edition.

1995). Figure 3c shows an example of a poorly coupled geophone housing on a rocky seafloor.

The first deployment (hereafter, DEPL1) took place between 6 July 2012 and 29 November 2012. It consisted of 12 instruments spaced 0.25–0.5 km apart at a water depth of 836 m (see Fig. 3a and Table S1). Only 11 instruments were retrieved, and they all recorded useful data. The tight spacing of this deployment was chosen for studies of the shallow sediment structure. The ability to locate regional or local earthquakes is very limited in this cluster geometry, and therefore we did not attempt to locate local earthquakes from this deployment. We used the data from DEPL1 only to investigate

ground-motion response from earthquakes cataloged and detected by land networks.

A second deployment (hereafter, DEPL2) of five OBS took place upon the retrieval of DEPL1 OBS (numbered hexagons in Fig. 2). DEPL2 consisted of five instruments with an internal spacing of about 55 km in an array covering the SNE continental margin at water depths between 815 and 2400 m (see Table S1). The OBSs were deployed from 29 November 2012 to 11 September 2013 and recorded useful data for 178 days (up to 26 May 2013). DEPL2 deployment geometry was designed to locate local earthquakes along the margin that were not detected by the land seismometers operating during this deployment.

We queried earthquake catalogs from the Incorporated Research Institutions for Seismology (IRIS), the NESN, the Lamont-Doherty Cooperative Seismographic Network (LCSN), U.S. Geological Survey, and the International Seismological Centre to search for all events that occurred during DEPL1 and DEPL2 time periods. In general, the local networks NESN and LCSN have a more comprehensive list of smaller magnitude earthquakes $M_{Lg} < 3.0$. Finally, for particular events of interest for the study of seismic attenuation of the continental margin, we also retrieved waveform data recorded at these land networks from the IRIS Data Management Center.

METHODS

We first investigated the detection limits of our deployments in terms of earthquake magnitude and distance. We searched through the land-based network catalogs for local and regional earthquakes to help define the minimum magnitude event that can be detected by both land networks and the OBS deployments (Fig. 2). Most events above magnitude 3 are listed in the NESN catalog by magnitude scale M_{Lg} (Ebel, 1994), whereas lower magnitudes events are listed by two other magnitude scales M_N and M_c (Ebel, 1982, 1994; Rosario, 1979). M_N uses the peak Lg wave of an earthquake measured at a specific period range, between 0.1 and 1.0 s (Ebel, 1994). M_c uses the coda duration of a recorded earthquake starting at the P -wave arrival to when the signal falls back to the background level (Rosario, 1979; Ebel, 1982). We sorted the events by M_c magnitudes and only used M_N magnitudes if an M_c magnitude was not available.

We then searched through the waveforms, recorded by the OBS to determine the minimum magnitude of onshore earthquake that could be detected by the OBS. Detections were determined by visible P and S arrivals in the waveforms. The waveforms were high-pass filtered with a corner period of 1.0 s. During DEPL1, one earthquake, magnitude of $M_c \sim 2.7 \pm 0.2$ at a distance ~ 325 km, was detected. The gray arc in Figure 2 marks the 325 km distance from DEPL1. A second earthquake M_{Lg} 4.5 located along coastal Maine was also detected. All other events during DEPL1 were not detected. A list of the events and their distances from DEPL1 OBS 3, the center of the deployment, used for this exercise is provided as Table S2.

Next, using earthquake detection tools (see [Data and Resources](#)) we searched for P - and S -wave arrivals in DEPL2 waveform database and associated the detected arrivals to local earthquakes. Given the expected small magnitudes of the earthquakes ($M_{Lg} \leq 3.0$), we filtered the data to a frequency band between 2 and 15 Hz. We searched for P and S waves in the 5–15 Hz and 2–10 Hz frequency bands, respectively. A long-to-short time-window ratio of 0.5–5.0 s was used to calculate a signal-to-noise ratio (SNR) that could be flagged for a potential arrival in the waveform database. We further imposed a SNR threshold of 2.5 to flag the signal as a potential arrival. With a complete database of detected triggers, we used a grid-search algorithm to associate the potential P and S arrivals with local earthquakes in time and space within the box outlined in Figure 2. The grid search utilized a standard 1D velocity model IASP-91 (Kennett and Engdahl, 1991) with epicenter depth tested every 2 km down to 25 km depth.

Nonearthquake noise dominates the frequency band expected for small magnitude events between 1 and 15 Hz. Webb (1998) and Olofsson (2010) show that ambient noise in OBSs can be the result of tides, marine animal vocalizations, ship traffic, and other man-made seismic sources. It is preferable to have a minimum of four stations with at least one arrival at each station (P or S) to locate an earthquake. However, because of the high level of noise in the frequency band of interest contributing to a high number of nonearthquake arrivals in the detection database, we needed to raise the threshold to reject the false positives of detected arrivals in our database. The detection criterion was raised to seven or more associated picks that could be attributed to an event. These groups of associations were then manually examined further to verify that the waveforms had the typical shape and frequency content for a local small-magnitude earthquake. Forty-seven total detected events, which do not appear in the various earthquake catalogs, satisfied the association criteria. Of those 47 detected events, only one event, however, satisfied the additional visual inspection criteria for an offshore earthquake event.

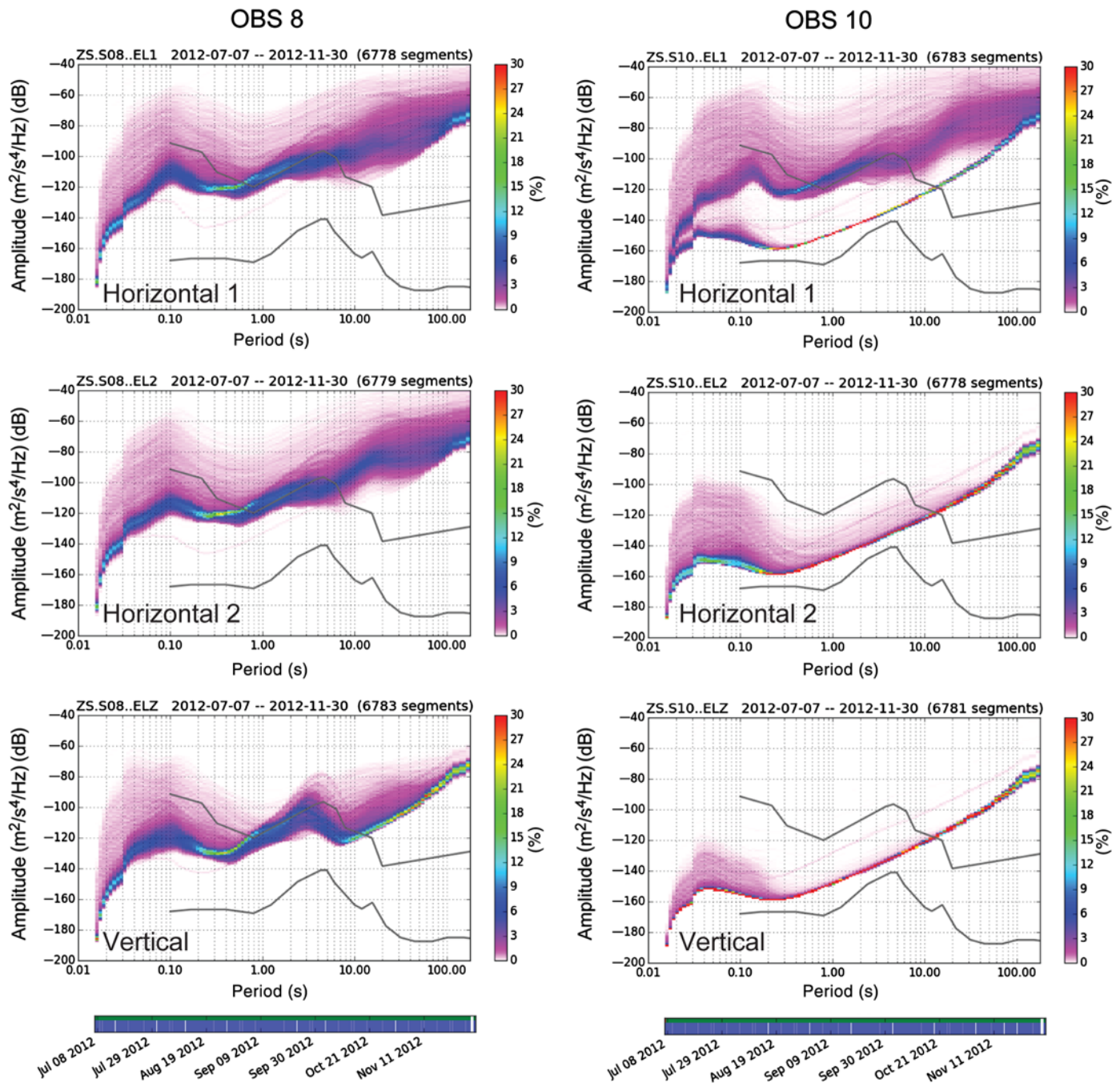
Very few, if any, ground-motion studies have used OBSs, due to the difficulty of differentiating between ground motion and the effects of instrument coupling to the ocean floor. Although there have been studies such as the site amplification near the Nankai trough (Nakamura *et al.*, 2014) and Scholte wave dispersion and waveform modeling at the Ninetyeast ridge (Nguyen *et al.*, 2009), we are not aware of similar studies done at the continental margin. The clustering of 11 instruments within 1–2 km of the seafloor during DEPL1 (Fig. 3a) allows for the comparison between instrument responses. If most of the instruments show similar responses, that response is assumed to represent the true ground motion and not instrument coupling, assuming little local variation in the subsurface.

To evaluate the reliability of the amplitude levels recorded by each OBS, we first removed its instrument response and then compared waveform amplitudes at each of the three components at both event and nonevent sections of the waveform. Two methods were used to evaluate the amplitude: (1) comparison of the background amplitude of the three components

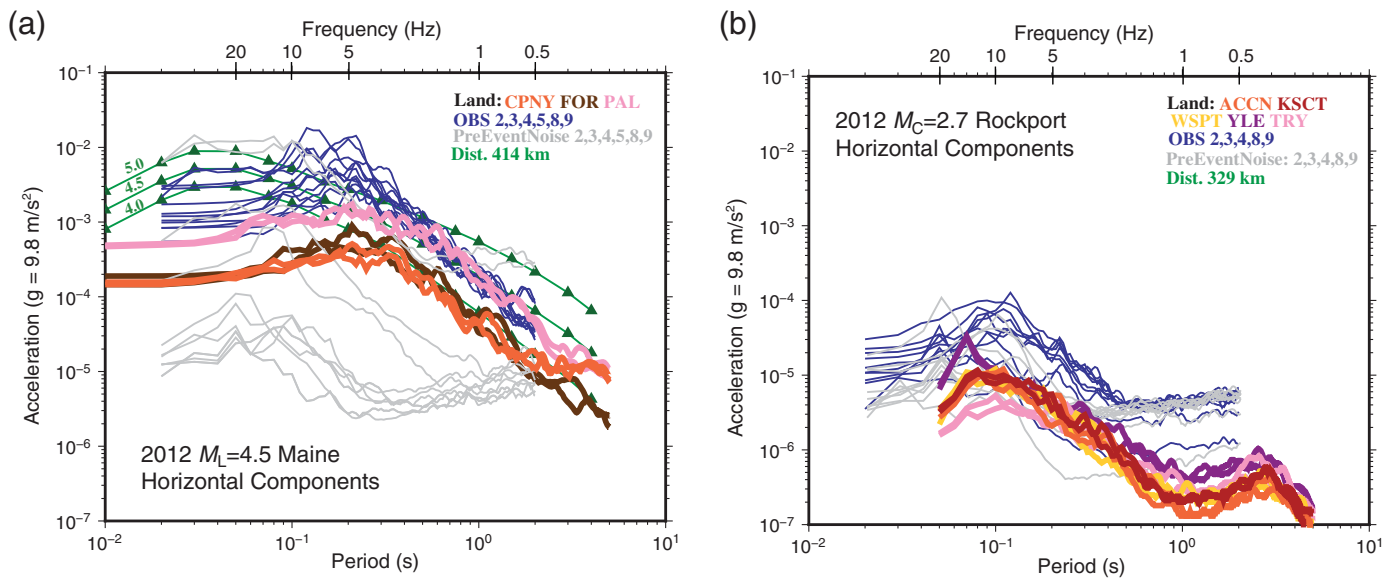
of the OBS, and (2) examination of the probability density function (PDF) plot of the power spectral density (PSD) for the whole time period of the deployment at each component of the OBS. In the first method, if an OBS had one component with amplitudes several orders of magnitude larger or smaller than another component in that same OBS, we classified that OBS as being bad. If all the components of the OBS were within the same order of magnitude, we classified that OBS as good. Using the second method, we generated PDF plots of the seismic PSD for the entire recording period using ObsPy (see [Data and Resources](#)). PDF plots are typically used to quantify the quality of data being recorded by land seismometers and reveal much about background noise levels recorded at a station (McNamara and Buland, 2004). The PDF plots (Fig. 4 and in the  electronic supplement to this article) reveal noise variations at each component of the OBS and the relative distribution of recorded frequencies through the recording period. The highest probability values, the darkest sections in these plots, show the median background noise of each station component.

The left column of Figure 4 is the seismic PSD of DEPL1 OBS 8 and has a very wide range of amplitudes throughout the plotted period range of the instrument, indicating that OBS 8 recorded the mean background noise and various other signals during its entire period of deployment. DEPL1 OBS 10 on the right column, however, has a smaller range of amplitudes plotted with a dramatic decrease in amplitude probability variability at periods greater than 0.2 s, indicating that two components of this OBS did not record much beyond its background noise. The right column plots also show lower noise amplitude than the left column plots. Because there is no significant difference in depth between the OBS, no gaps and the distance between them is only ~ 1 km, it is more likely that the DEPL1 OBS 10 suffered from poor coupling to the ocean floor rather than being the result of a site effect. With these discriminants in mind, we used the subset of good OBS (i.e., OBS with reliable amplitudes) for further study of the attenuation of the continental margin. Based on the above criteria, our list of good OBS during DEPL1 is 2, 3, 4, 5, 8, and 9.

To calculate the attenuation in the continental margin, we adapted the McNamara *et al.* (2012, 2014) method to the OBS data, which was previously applied to study the seismic attenuation from the 2010 Haiti and the 2011 Virginia earthquakes. Our data do not have an extensive collection of recorded earthquakes, especially during DEPL1. Therefore, we are not able to carry out a complete attenuation study as was done in Virginia and Hispaniola. Instead, we compared the amplitudes from two events less than 15° away from DEPL1, which were recorded on the OBS and on selected land stations. The OBS waveforms were first filtered between 0.1 and 45 Hz, converted to acceleration, then cropped to just before the arrival of the P wave (8.1 km/s) to after the surface waves (2.0 km/s) as input for the PSA calculation with 5% damping. We identified the SA of each event for periods between 0.05 and 2.0 s to be 20–0.5 Hz. We also examined the internal consistency of the SA of the two horizontal components of previously determined good



▲ **Figure 4.** Probability density function (PDF) plots of the power spectral density (PSD) for two OBS stations from DEPL1. A time-increment bin of 3600 s (1 hr) is used to calculate the PSD. OBS components: EL1, horizontal 1; EL2, horizontal 2; and ELZ, vertical. The left column shows an example of an OBS with good quality data for the entire time of the deployment, OBS 08. The right column shows an example of an OBS with bad quality data in two of its components; EL2 and ELZ and some bad data in EL1 for the entire time of the deployment, OBS 10. The two solid lines show the high- and low-noise models from the measurement of Global Seismic Network (GSN) stations from [Peterson \(1993\)](#). The scale bar to the right shows the probability that the recorded data will fall within a certain power spectral level at a given frequency for the entire time span. The highest probability values, warm colors in the online color version of Figure 4 and [E](#) electronic supplement, show the median background noise of the station component. The bar with dates below the plot shows the time span of the data collected during DEPL1 included in the PSD. In the online color version, the top row shows data input into the PSD, green patches represent available data, and red patches represent gaps in the input that were added to the PSD. The bottom row in blue shows the single PSD measurements that go into the histogram. Because the default processing method fills gaps with zeros, these data segments then show up as single outlying PSD lines ([Beyreuther et al., 2010](#)). See [McNamara and Buland \(2004\)](#) for further background on the interpretation of PDFs. The color version of this figure is available only in the electronic edition.



▲ **Figure 5.** (a) Horizontal acceleration spectra plot for the 2012 M_{Lg} 4.5 Maine earthquake. The horizontal components of the good OBS from DEPL1 are shown in thin dark lines and the horizontal components of the land accelerometers at CPNY, FOR, and PAL from the Lamont-Doherty Cooperative Seismographic Network (LCSN) shown in heavy lines. Pre-event noise spectra for the OBS are shown as thin gray lines. The length of the pre-event window analyzed for its spectra is equal to the length of the event window. The locations of the earthquake and corresponding stations are shown in Figure 2. For reference, the Campbell (2003) predicted peak spectral accelerations are shown as curves with triangles each labeled with their corresponding magnitudes for a distance of 415 km. Distances and azimuths from the earthquake for all the stations are listed in Table S3. Y axis is acceleration in units of $g = 9.8 \text{ m/s}^2$. (b) Horizontal acceleration spectra plot for the 2012 $M_c = 2.7$ Rockport earthquake. The horizontal components of the good OBS from DEPL1 are shown in thin dark lines, and the horizontal components of the land seismometers at ACCN, KSCT from the LCSN, and TRY, WSPT, YLE from the NESN are shown in heavy lines. Pre-event noise spectra for the OBS are shown as thin gray lines. The length of the pre-event window analyzed for its spectra is equal to the length of the event window. The locations of the earthquake and corresponding stations are shown in Figure 2. Distances and azimuths from the earthquake for all the stations are listed in Table S4. Y axis is acceleration in units of $g = 9.8 \text{ m/s}^2$. The color version of this figure is available only in the electronic edition.

versus bad OBS. The SA-derived classification was consistent with the amplitude-based classification of the entire record, discussed above, except for when noise that occurred during an earthquake arrival biased the SA calculation of that OBS. Figure 5a and 5b shows the comparison of all the DEPL1 OBS horizontal SAs for the two events identified, Maine-2012 and Rockport-2012, respectively. We normalized the SA value to gravity, $g = 9.8 \text{ m/s}^2$. For the Rockport-2012 earthquake, OBS 5 has short-period noise conflicting with the earthquake arrivals and therefore is not included in Figure 5b. The land stations, used for comparison with the OBS SA, had similar distance ranges to the distance between the earthquake and DEPL1 (see Tables S3 and S4). SA calculation for the Maine-2012 earthquake utilized available accelerometer data from the land stations. Only seismometer data were available for the Rockport-2012 earthquake, and these had to be converted to acceleration for the SA calculation.

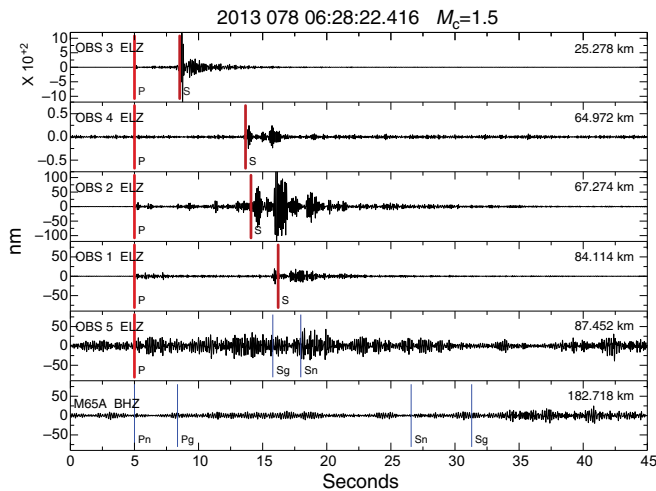
We compared our calculated ground motions from the Maine-2012 earthquake to the Campbell (2003) ground-motion model for the eastern United States, bearing in mind that his model was developed to predict ground motion for earthquakes $M_{Lg} > 5.0$, whereas the Maine earthquake was M_{Lg} 4.5. In addition, other factors such as source, site response, radi-

ation pattern, and directivity may contribute to the scatter of computed SA up to an order of magnitude (Atkinson, 2012).

RESULTS

Offshore Earthquakes Not Reported by the Land Arrays

During the entire period of DEPL2, only one earthquake was detected from an actual offshore location that was not reported by the catalogs (Table S5) but can be seen by some of the land seismometers, the star near deployed OBS in Figure 2. The vertical-component waveforms for the OBS and one land station are shown in Figure 6, whereas the rest of the waveforms are presented in Figure S9a–c. The event on 19 March 2013 (Julian Date [JD] 078) 06:28:22.42 was located at (-71.3767° W , 40.0131° N , depth = 15.72 km). It was detected by all five OBS in DEPL2 with 10 detected arrivals. Following NESN method of M_c calculation (Rosario, 1979), we used the average coda time length from four stations to determine a magnitude of $M_c = 1.5 \pm 0.4$. Only one land station had a clear recording of the P and S waves, WSPT in Westport, Connecticut, at a distance of 209 km, whereas several others only recorded surface waves from this earthquake (Fig. S9b). USArray station M65A located in Falmouth, Massachusetts,



▲ **Figure 6.** Vertical-component (ELZ) waveforms from DEPL2 OBS of the identified local event 19 March 2013 (JD 078), 06:28:22.416. See location indicated as a star near the OBS deployments in Figure 2. The bottom vertical waveform (BHZ) is from USArray station M65A located in Falmouth, Massachusetts (labeled triangle in Fig. 2). The waveforms are plotted in order of distance from the earthquake with distance in kilometers indicated on the top right corner of each waveform. All waveforms have been Butterworth-band-pass filtered between 5 and 15 Hz. Heavy lines show P and S arrivals that were detected and used for determining earthquake location. S arrivals were actually picked on the horizontal components and are being projected onto the vertical component in this plot. Thin lines with labeled arrivals (P_n , P_g , S_n , and S_g) indicate predicted arrivals using IASP-91 velocity model (Kennett and Engdahl, 1991). The color version of this figure is available only in the electronic edition.

almost 183 km away (labeled triangle in Fig. 2) was the nearest land-based instrument, but the P and S arrivals were not detectable above the noise in the waveform from M65A (bottom waveform in Fig. 6). Permanent regional stations, which detected S waves from this small event include WSPT, BRYW, FOR, CPNY, PAL, KSCT, WES, QUA2, BRNY, BRNJ, ODNJ, NPNY, TUPA, and FFD, located between Massachusetts and New Jersey (waveforms are provided in the electronic supplement).

Seismic Attenuation of the Continental Margin

A significant New England earthquake occurred on land near the coast of Maine on 16 October 2012, 23:12:22.29 UTC with an $M_{Lg} \sim 4.5$. Although other significant regional earthquakes took place during both deployments, such as the 17 May 2013 M_{Lg} 4.5 Quebec earthquake, their epicenters were far from shore. These earthquakes were not considered in this study because the majority of their propagation path to the OBS was on land, not within the margin. The location and size of this earthquake provided a rare opportunity compare an on-land and a continental-margin path. We took advantage of work by Herrmann *et al.* (2011) in calculating earthquake source parameters for smaller magnitude earthquakes ($M < 5.5$) using

permanent land seismic networks and the deployed USArray instruments. The Maine-2012 earthquake was calculated to have a magnitude of M_w 4.03 with a depth of 7 km and a thrust fault focal mechanism (Herrmann *et al.*, 2011) shown in Figure 2 (see Data and Resources). The average distance to the DEPL1 OBS from this event is 415 km. The earthquake recorded on all the OBS components including the hydrophone. The SA from this event, calculated from the good quality OBS cluster, is plotted together with the predicted attenuation curve of Campbell (2003; Fig. 5a). We also plotted for comparison of the calculated SA for three land accelerometers in New York (locations shown in Fig. 2), located at similar distances from the event as the OBS (Table S3). The azimuthal variation of the propagation path between the OBS cluster and the land accelerometers differs by only 30°–40°.

We also studied the offshore Rockport 16 September 2012 (JD 260) 02:31:37.6, $M_c = 2.7$, $M_N = 2.5$ and compared the calculated SA from DEPL1 to SA calculated for five land seismometers (location shown in Fig. 2 and plot in Fig. 5b). The propagation path to the land seismometers and to the DEPL1 differs by 45°–90° (Table S4).

Figure 5a shows that at least for a propagation path along the shelf and upper slope of SNE, the seismic attenuation of the continental shelf is similar to that for an on-land propagation path in coastal New York and New England. The attenuation observed on the land instruments in the 4–10 Hz frequency band is an order of magnitude higher than that observed on the OBS, perhaps because of cultural noise in the New York area. The presence of 2–3 km of sediments under the OBS DEPL1 tapering to ~100 m south of Cape Cod did not seem to have a significant effect on the SA. This is perhaps due to the relatively high wavespeed of the mostly lithified sediments on the shelf and the location of DEPL1 within a landslide scar, at which the overlying unconsolidated sediments have probably been removed (Fig. 3a). The SA from the OBS is somewhat similar to the predicted SA of Campbell (2003) for the eastern United States, although there are differences at frequencies 2–10 Hz. It is worth noting that the site shear-wave velocity in Campbell's model is assumed to be 2800 m/s, higher than for the sediments underlying DEPL1 (~400 m/s; N. C. Miller, personal comm., 2016).

The SA of the land seismometers from the Rockport-2012 earthquake is an order of magnitude lower than that from DEPL1 OBS. This may be due to the propagation path that is perpendicular to the fabric of the Appalachian orogenies.

Despite the lack of control on OBS placement, looking at the SA of the two earthquakes, the OBS seems to record motions significantly higher by almost a factor of 10 compared to the land stations (Fig. 5). This could be the result of more efficient wave propagation within the continental shelf or be due to a site effect.

The spectrum immediately prior to the P -wave arrival time for each event was calculated to estimate pre-event noise (thin gray lines in Fig. 5). The length of the pre-event window was similar to that of the following event windows, 157 s for the Maine earthquake and 124 s for the Rockport earthquake.

The time-window lengths correspond to the respective time windows used for the SA calculation of each earthquake. The noise spectrum for the 2012 Maine earthquake is 1–2 orders of magnitude less than the earthquake SA for frequencies < 10 Hz (Fig. 5a) but is only slightly smaller than the SA for the Rockport earthquake. Hence, the SA at 4–10 Hz may reflect path attenuation and site conditions (Fig. 5a), but the SA > 10 Hz (Fig. 5b) may reflect the ambient noise spectrum. Data used for the spectral acceleration are included in the supplement.

DISCUSSION AND CONCLUSIONS

Data recorded by two short-period OBS networks 150–200 km offshore New York and SNE reveal the detection limits and attenuation structure of the margin. Only one $M_c = 1.5$ earthquake, detected by the OBS array during the six months deployment, was not listed by any of the regional catalogs, although further inspection showed that S waves from these earthquakes were recorded by several land stations. Hence, microearthquake activity of this margin is probably successfully monitored by land seismometers without the need for OBS deployments. Because earthquakes with magnitudes of $M_{Lg} < 4.0$ – 5.0 are generally incapable of generating landslides (Keefe, 1994; ten Brink *et al.*, 2014), a land-based network is likely to detect earthquakes capable of generating tsunamigenic landslides along the U.S. Atlantic coast.

The SA from an $M_{Lg} 4.5$ earthquake 415 km away from the OBS cluster and from land accelerometers at a similar distance appear similar, indicating that the seismic attenuation of the margin is similar to that of the eastern seaboard. Furthermore, for the $M_{Lg} 4.5$ earthquake, both the OBS and the land station are similar to the Campbell (2003) SA model for the eastern United States. For the $M_c = 2.7$ Rockport earthquake, land stations ~320 km away from the epicenter have higher attenuation than the OBS at similar distances, perhaps because the propagation path to these stations is perpendicular to the geologic structure of the Appalachians, whereas the path to the OBS is parallel to the structure. The peak ground acceleration of the OBS between frequencies 3 and 10 Hz for the $M_{Lg} 4.5$ Maine earthquake is shifted to lower frequencies versus those from the Rockport earthquake, reflecting the earthquake frequency content difference between both events. The SA for the Rockport earthquake is only slightly higher than the pre-event noise at frequencies > 3 Hz, likely because the frequency content of small earthquakes is shifted toward higher frequencies. Both pre-event noise spectra show noise content to be concentrated above 10 Hz. The background noise does not explain the peaks seen between 5 and 10 Hz in the Maine earthquake. The Rockport event plots above the background noise only for a very small set of frequencies (3–10 Hz). The analysis reported in this article suggests that the seismic attenuation structure of the eastern seaboard in the New York–SNE area can be extended eastward to the continental slope. Similar studies elsewhere along the margin will help extend the seismic-hazard maps into the continental margins of the United States.

DATA AND RESOURCES

The data were recorded by instruments from the Ocean-Bottom Seismograph Instrument Pool (OBSIP; <http://www.obsip.org>, last accessed July 2016), which is funded by the National Science Foundation (NSF) and by the U.S. Geological Survey (USGS). OBSIP D2 instrument specifications can be found at <http://www.obsip.org/instruments/short-period/whoi/specifications/> (last accessed July 2016). Data are archived at the Incorporated Research Institutions for Seismology Data Management Center (IRIS-DMC; <http://www.iris.edu>, last accessed July 2016), listed under ZS(2012-2013) Seismicity of the East Coast Submarine Landslides is listed at http://dx.doi.org/10.7914/SN/ZS_2012 (last accessed July 2016). The IRIS-DMC was used to access waveforms, related metadata, and (or) derived products used in this study. IRIS Data Services are funded through the Seismological Facilities for the Advancement of Geoscience and EarthScope (SAGE) Proposal of the NSF under Cooperative Agreement EAR-1261681. Data from the International Seismological Centre (ISC) were accessed from their *online bulletin* International Seismological Center, Thatcham, United Kingdom, 2015 (<http://www.isc.ac.uk>; last accessed April 2016). Data from Lamont-Doherty Cooperative Seismographic Network (LCSN) can be found at <http://www.fdsn.org/networks/detail/LD> (last accessed April 2016). Data from the New England Seismic Network (NESN) are available at <http://dx.doi.org/10.7914/SN/NE> (last accessed April 2016). Data from the Transportable Array (TA) network were made freely available as part of the EarthScope USArray facility, operated by IRIS and supported by the NSF, under Cooperative Agreements EAR-1261681. Data on the Maine-2012 earthquake are taken from the Saint Louis University (SLU) Digital Data Focal Mechanism Pages available at http://www.eas.slu.edu/eqc/eqc_mt/MECH.NA/index.html (last accessed April 2016). Antelope 5.4 was used for processing waveform data for earthquake detection and location. Some maps were made using ArcGIS 10.1 (www.esri.com, last accessed April 2016). Some plots were made using Generic Mapping Tools v4.2.1 (www.soest.hawaii.edu/gmt/, last accessed April 2016; Wessel *et al.*, 2013). ObsPy 1.0.1 software was used for processing waveform data (<https://www.obspy.org/>, last accessed July 2016; Beyreuther *et al.*, 2010). Waveforms plotted for publication were made using Seismic Analysis Code v.101.6a (<http://www.iris.edu>, last accessed April 2016). Original map of Figure 1 is located at https://akafka.files.wordpress.com/2014/02/neus_network_seis_sm2.png (last accessed April 2015). ✉

ACKNOWLEDGMENTS

We would like to thank Daniel McNamara for his thoughtful internal review that greatly improved this article. We also want to thank John Ebel, Richard Lee, and two other reviewers for their insightful comments and suggestions. Conversations with Nathaniel Miller were also helpful. This project was partially funded by the Nuclear Regulatory Commission under NRC Job Number V6166. Any use of trade, firm, or product names

is for descriptive purposes only and does not imply endorsement by the U.S. Government.

REFERENCES

- Andrews, B. D., J. D. Chaytor, U. S. ten Brink, D. S. Brothers, and J. V. Gardner (2013). Bathymetric terrain model of the Atlantic margin for marine geological investigations, *U.S. Geol. Surv. Open-File Rept. 2012-1266*, doi: [10.3133/ofr20121266](https://doi.org/10.3133/ofr20121266).
- Atkinson, G. M. (2012). Evaluation of attenuation models for the northeastern United States/southeastern Canada, *Seismol. Res. Lett.* **83**, no. 1, 166–178, doi: [10.1785/gssrl.83.1.166](https://doi.org/10.1785/gssrl.83.1.166).
- Beyreuther, M., R. Barsch, L. Krischer, T. Megies, Y. Behr, and J. Wassermann (2010). ObsPy: A Python toolbox for seismology, *Seismol. Res. Lett.* **81**, no. 3, 530–533, doi: [10.1785/gssrl.81.3.530](https://doi.org/10.1785/gssrl.81.3.530).
- Campbell, K. W. (2003). Prediction of strong ground motion using the hybrid empirical method and its use in the development of ground-motion (attenuation) relations in eastern North America, *Bull. Seismol. Soc. Am.* **93**, no. 3, 1012–1033, doi: [10.1785/0120020002](https://doi.org/10.1785/0120020002).
- Chaytor, J., U. S. ten Brink, A. R. Solow, and B. D. Andrews (2009). Size distribution of submarine landslides along the U.S. Atlantic margin, *Mar. Geol.* **264**, nos. 1/2, 16–27, doi: [10.1016/j.margeo.2008.08.007](https://doi.org/10.1016/j.margeo.2008.08.007).
- Duennebie, F. K., and G. H. Sutton (1995). Fidelity of ocean bottom seismic observations, *Mar. Geophys. Res.* **17**, no. 6, 535–555, doi: [10.1007/BF01204343](https://doi.org/10.1007/BF01204343).
- Ebel, J. E. (1982). M_L measurements for northeastern United States earthquakes, *Bull. Seismol. Soc. Am.* **72**, no. 4, 1367–1378.
- Ebel, J. E. (1994). The $M_{Lg}(F)$ magnitude scale: A proposal for its use northeastern North America, *Seismol. Res. Lett.* **65**, no. 2, 157–166, doi: [10.1785/gssrl.65.2.157](https://doi.org/10.1785/gssrl.65.2.157).
- Grilli, S. T., O.-D. S. Taylor, D. P. Baxter, and S. Maretzki (2009). Probabilistic approach for determining submarine landslide tsunami hazard along the upper East Coast of the United States, *Mar. Geol.* **264**, nos. 1/2, 74–97, doi: [10.1016/j.margeo.2009.02.010](https://doi.org/10.1016/j.margeo.2009.02.010).
- Herrmann, R. B., H. Benz, and C. J. Ammon (2011). Monitoring the earthquake process in North America, *Bull. Seismol. Soc. Am.* **101**, no. 6, 2609–2625, doi: [10.1785/0120110095](https://doi.org/10.1785/0120110095).
- Keefer, D. K. (1994). The importance of earthquake-induced landslides to long-term slope erosion and slope-failure hazards in seismically active regions, *Geomorphology* **10**, nos. 1/4, 265–284, doi: [10.1016/0169-555X\(94\)90021-3](https://doi.org/10.1016/0169-555X(94)90021-3).
- Kennett, B. L. N., and E. R. Engdahl (1991). Traveltimes for global earthquake location and phase identification, *Geophys. J. Int.* **105**, no. 2, 429–465, doi: [10.1111/j.1365-246X.1991.tb06724.x](https://doi.org/10.1111/j.1365-246X.1991.tb06724.x).
- Kim, W.-Y. (1998). The M_L scale in eastern North America, *Bull. Seismol. Soc. Am.* **88**, no. 4, 935–951.
- McNamara, D. E., and R. P. Buland (2004). Ambient noise levels in the continental United States, *Bull. Seismol. Soc. Am.* **94**, no. 4, 1517–1527, doi: [10.1785/012003001](https://doi.org/10.1785/012003001).
- McNamara, D. E., L. Gee, H. M. Benz, and M. Chapman (2014). Frequency-dependent seismic attenuation in the eastern United States as observed from the 2011 central Virginia earthquake and after-shock sequence, *Bull. Seismol. Soc. Am.* **104**, no. 1, 55–72, doi: [10.1785/0120130045](https://doi.org/10.1785/0120130045).
- McNamara, D., M. Meremonte, J. Z. Maharrey, S.-L. Mildore, J. R. Altidore, D. Anglade, S. E. Hough, D. Given, H. Benz, L. Gee, and A. Frankel (2012). Frequency-dependent seismic attenuation within the Hispaniola Island region of the Caribbean Sea, *Bull. Seismol. Soc. Am.* **102**, no. 2, 773–782, doi: [10.1785/0120110137](https://doi.org/10.1785/0120110137).
- Nakamura, T., M. Nakano, N. Hayashimoto, N. Takahashi, H. Takenaka, T. Okamoto, E. Araki, and Y. Kaneda (2014). Anomalously large seismic amplifications in the seafloor area off the Kii peninsula, *Mar. Geophys. Res.* **35**, 255–270, doi: [10.1007/s11001-014-9211-2](https://doi.org/10.1007/s11001-014-9211-2).
- Nguyen, X. N., T. Dahm, and I. Grevemeyer (2009). Inversion of Scholte wave dispersion and waveform modeling for shallow structure of the Ninetyeast ridge, *J. Seismol.* **13**, 543–559, doi: [10.1007/s10950-008-9145-8](https://doi.org/10.1007/s10950-008-9145-8).
- Olofsson, B. (2010). Marine ambient seismic noise in the frequency range 1–10 Hz, *The Leading Edge* **29**, no. 4, 418–435, doi: [10.1190/1.3378306](https://doi.org/10.1190/1.3378306).
- Peterson, J. R. (1993). Observation and modeling of seismic background noise, *U.S. Geol. Surv. Open-File Rept.* 93-322, 94 pp.
- Peterson, M. D., M. P. Moschetti, P. M. Powers, C. S. Mueller, K. M. Haller, A. D. Frankel, Y. Zeng, S. Rezaeian, S. C. Harmsen, O. S. Boyd, et al. (2014). Documentation for the 2014 update of the United States National Seismic Hazard Maps, *U.S. Geol. Surv. Open-File Rept. 2014-1091*, 243 pp., doi: [10.3133/ofr20141091](https://doi.org/10.3133/ofr20141091).
- Poag, C. W., and W. D. Sevon (1989). A record of Appalachian denudation in posttrifurcated Mesozoic and Cenozoic sedimentary deposits of the U.S. Middle Atlantic continental margin, *Geomorphology* **2**, nos. 1/3, 119–157, doi: [10.1016/0169-555X\(89\)90009-3](https://doi.org/10.1016/0169-555X(89)90009-3).
- Rosario, M. (1979). A coda duration magnitude scale for the New England Seismic Network, *Master's Thesis*, Boston College, Chestnut Hill, Massachusetts, 82 pp.
- Tavakoli, B., and S. Pezeshk (2005). Empirical-stochastic ground-motion prediction for eastern North America, *Bull. Seismol. Soc. Am.* **95**, no. 6, 2283–2296, doi: [10.1785/0120050030](https://doi.org/10.1785/0120050030).
- ten Brink, U. S., R. Barkan, B. D. Andrews, and J. D. Chaytor (2009). Size distributions and failure initiation of submarine and subaerial landslides, *Earth Planet. Sci. Lett.* **287**, nos. 1/2, 31–42, doi: [10.1016/j.epsl.2009.07.031](https://doi.org/10.1016/j.epsl.2009.07.031).
- ten Brink, U. S., J. D. Chaytor, E. L. Geist, D. S. Brothers, and B. D. Andrews (2014). Assessment of tsunami hazard to the U.S. Atlantic margin, *Mar. Geol.* **353**, 31–54, doi: [10.1016/j.margeo.2014.02.011](https://doi.org/10.1016/j.margeo.2014.02.011).
- ten Brink, U. S., H. J. Lee, E. L. Geist, and D. Twichell (2009). Assessment of tsunami hazard to the U.S. East Coast using relationships between submarine landslides and earthquakes, *Mar. Geol.* **264**, nos. 1/2, 65–73, doi: [10.1016/j.margeo.2008.05.011](https://doi.org/10.1016/j.margeo.2008.05.011).
- Webb, S. C. (1998). Broadband seismology and noise under the ocean, *Rev. Geophys.* **36**, no. 1, 105–142, doi: [10.1029/97RG02287](https://doi.org/10.1029/97RG02287).
- Wessel, P., W. H. F. Smith, R. Scharroo, J. F. Luis, and F. Wobbe (2013). Generic Mapping Tools: Improved version released, *Eos Trans. AGU* **94**, no. 45, 409–410, doi: [10.1002/2013EO450001](https://doi.org/10.1002/2013EO450001).

Claudia H. Flores

Uri S. ten Brink

U.S. Geological Survey

Woods Hole Coastal and Marine Science Center

384 Woods Hole Road

Woods Hole, Massachusetts 02543-1598 U.S.A.

cflores@usgs.gov

utenbrink@usgs.gov

Jeffrey J. McGuire

John A. Collins

Geology and Geophysics Department

Woods Hole Oceanographic Institution

266 Woods Hole Road, MS# 24

Woods Hole, Massachusetts 02543-1050 U.S.A.

jm McGuire@whoi.edu

jcollins@whoi.edu

Published Online 2 November 2016